DOI: 10.13009/EUCASS2023-580
Aerospace Europe Conference 2023 – 10TH EUCASS – 9TH CEAS

Application of a deep neural network for C_p prediction on multiple wing geometries in a transonic regime

Alejandro Gorgues[⋆†], *R. Castellanos*[⋆], *J. Nieto-Centenero*[⋆‡] *and E. Andrés-Pérez*[⋆]

[⋆]Theoretical and Computational Aerodynamics Branch, Flight Physics Department
Instituto Nacional de Técnica Aeroespacial (INTA)
Ctra. Ajalvir Km.4 Torrejón de Ardoz 28850, España.

[†]Escuela Politécnica Superior
Universidad de Alcalá de Henares (UAH)
28805 Alcalá de Henares, España.

[‡]Escuela Técnica superior de Ingeniería Aeronáutica y del Espacio (ETSIAE)
Universidad Politécnica de Madrid (UPM)
28223 Madrid, España.

gorguesva@inta.es · rcasgar@inta.es · jniecen@inta.es · eandper@inta.es

Abstract

The aerospace industry has embraced data-driven methods for aerodynamic shape optimization to reduce costs. Surrogate models have been used to provide reasonably accurate results in less time compared to Computational Fluid Dynamics (CFD) simulations and machine learning techniques have been applied to the aerodynamic shape optimization of complex cases. In this paper, a Deep Neural Network (DNN) is used to predict the pressure coefficients (C_p) of transonic wings, given flight conditions and geometric parameters. The results show that the prediction values are close to the values calculated with CFD simulations, although some errors appear in the case of non-linear phenomena related to shockwaves.

1. Introduction

Aerodynamic shape optimisation based on CFD simulations has been widely used in aircraft design due to its maturity level. This optimisation typically involves treating a huge amount of data that come from a space based on flight conditions and/or geometrical configurations. Given the amount of variability of parameters employed, a high dimensionality space can slow down the process; for that, surrogate models can be used jointly to accelerate it.

As stated by Yondo et al. [1], different surrogate-based modeling approaches have been applied to aerodynamic data to support the analysis and optimization of aircraft design. For example, in Andrés and Paulete-Periáñez [2] an airfoil comparison has been made on three aeronautical configurations to predict lift and drag coefficients. Among all of them, artificial neural networks have emerged as an alternative to model data and extract its non-linearity, whose architectures may vary according to the objective to be pursued. For example, to predict aerodynamic coefficients, Moin et al. [3] uses a multi-layer perceptron (MLP) architecture; to improve the shape optimisation process, Yonekura and Suzuki [4] implements a conditional variational autoencoder (CVAE); or Li et al. [5] developed a composition of a convolutional generative adversarial network (DCGAN) and a convolutional neural network (CNN) due to the appearance of the curse of dimensionality.

In the field of aerodynamics, there is a complexity associated with obtaining data, as the process can be very expensive and time-consuming. By default, neural networks cannot identify the error or uncertainty quantification [6]. Therefore, under complex environments such this one, it is often necessary to use datasets that may contain noisy information in order to address this objective. The provision of uncertainty quantification techniques into the data for training, as well as its robustness analysis, is an important aspect to take into account, which has been applied to other fields. Shahzadi and Soulaïmani [7], for example, employs a polynomial chaos expansion surrogate model to analyse the displacement sensitivity of the soil from a rockfill dam. More specifically, since the uncertainty can come from the model or from the data, a different family of methods can be applied to its understanding [8].

DOI: 10.13009/EUCASS2023-580

Table 1: Definition of the different flight conditions and geometric features used to build the database. A total of 56 flight conditions and 60 wing geometries, summing up 3 360 simulations.

Flight condition		Geometric features	
α	0°, 2°, 3°, 4°, 5°, 6°, 7°, 8°	b/b_0	0.9, 1.0, 1.1, 1.2
M	0.70, 0.74, 0.78, 0.80, 0.82, 0.84, 0.86	$\Delta\Lambda$	-5°, -2°, 0°, +2°, +5°
		t/t_0	0.9, 1.0, 1.1

A way to evaluate the performance of the model, is to study the propagation of uncertainty in terms of normal noise injection into the inputs to investigate what outputs the model produced. For example, Ziyadinov and Tereshonok [9] performed a robustness characterisation of different linear classifiers under multiple random noise models, where one of them is modelled as a Gaussian distribution. In another research, by Silva and Adeodato [10], Gaussian noise has been added after a PCA transformation of the variables for predictive analysis of different data sets. Furthermore, it has also been used to study how noise injection is able to regularise values in regression and classification under a Fourier space, as indicated by Camuto et al. [11].

This research describes an approach to the analysis of the robustness of a DNN architecture in different geometrical wing configurations and flight conditions. For the study of the noise stability of the model, a process where noise data is created based on a Gaussian distribution is gonna be tested against it and analysed as well.

This paper is structured as follows. First, we describe the methodology in Section 2, starting with a mathematical introduction of the Deep Neural Network and how it is applied to the database. Then, the measurement of the robustness of the model is commented on. Therefore, an explanation of the results obtained will be displayed in Section 3 and finally, the conclusions are enumerated in Section 4.

2. Methodology: building and analysis the surrogate model

In this section, an explanation of the methodology and database utilised in this study is provided. It begins by presenting an overview of the database and the model geometry being examined. After that, a summary of the Deep Neural Network employed is given, along with an analysis of the parameter selection, tuning process and the evaluation of the robustness of the model.

2.1 Database and test case

The database used for the present research is composed by CFD simulations of the XRF1 wing 3D model operating in the transonic regime. The XRF1 model is specifically designated by Airbus as a test case to showcase the implementation of various technologies for long-range wide-body aircraft. This research was carried out within the GARTEUR AD/AG60 European research project [12].

In these simulations, a simplified version of the XRF1 wing geometry derived from the original Computer Aided Design (CAD) model, is employed, where the Flap Track Fairing (FTF) and the engine were removed previously. However, several geometric modifications are allowed relative to the baseline design (represented as the subscript '0'). These modifications include variations in the wing-span ratio b/b_0, the sweep angle increment $\Delta\Lambda$ ($\Lambda - \Lambda_0$), and the thickness ratio t/t_0. A total of 60 different wing geometries are simulated, each using a structured mesh composed of 6 519 grid points distributed across 41 wing sections, as depicted in Figure 1. Table 1 presents a summary of the flow and geometric characteristics, including their respective intervals. Furthermore, Figure 2 illustrates the sketched representations of the geometric variations.

The aerodynamic data analysed in this study, which has been used also by Castellanos et al. [13] who proposes a data-driven surrogate model to be used in the preliminary design process using Isometric Feature Mapping (Isomap), is obtained from computational simulations using *RapidCFD* software, which implements the BLWF code developed at the Central Aerohydrodynamic Institute (TsAGI) [14, 15]. The BLWF code solves the boundary-value problem for the complete velocity-potential equation, considering the viscosity within the boundary layer approximation while maintaining a fixed position for the transition from laminar to turbulent flow. This approach effectively captures local supersonic areas, shock waves, and flows with small separation zones. Extensive verification of the method has demonstrated its high reliability.

The database contains a total of 3 360 simulations, combining various flight conditions and geometric alterations outlined in Table 1. For each simulation, the pressure coefficient (C_p) has been computed on the wing surface. The resulting data is incorporated onto a common structured grid mentioned previously. The 3 360 cases that make up the database have been divided into two sets: the *training* set (70% of the database) used to train the DNN, and the *test* set

DOI: 10.13009/EUCASS2023-580

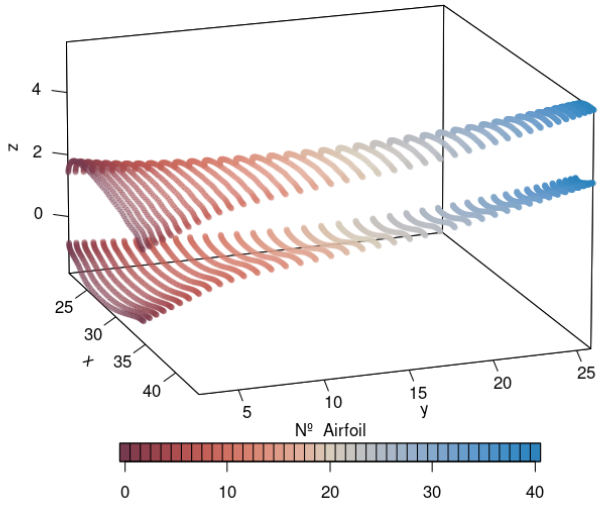

Figure 1: Wing mesh representation with the upper and lower side divided for better representation

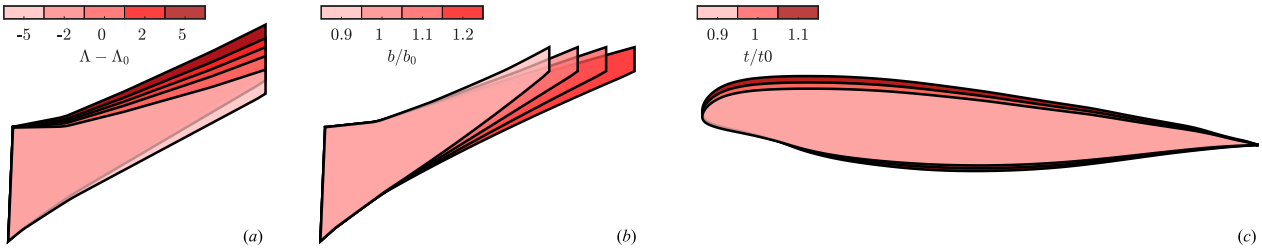

Figure 2: Schematic representation of the different geometric parameters used to generate the database. The geometric parameters (denoted with subscript 0), describes an alteration of the nominal geometry, which are: (a) Increment of sweep angle $\Delta\Lambda = \Lambda - \Lambda_0$ in degrees, (b) scaling of the wing span b/b_0, and (c) scaling of thickness ratio t/t_0.

with all the remaining cases (30% of the database) to evaluate the trained surrogate model, assessing its capability to interpolate C_p throughout the design space. The cases within the *test* set are never considered for training the DNN. For now, two cases within the *test* set are chosen for visualisation purposes (C_1 $\{M, \alpha, \Delta\Lambda, t/t_0, b/b_0\} = \{0.86, 6, -2, 1.1, 1.1\}$ and C_2 $\{M, \alpha, \Delta\Lambda, t/t_0, b/b_0\} = \{0.7, 7, 2, 1.1, 1.2\}$) due to the presence of shock waves, as they are challenging for the surrogate model.

To determine the significance of the features and the CFD data, the correlation between these features and the average and root mean square of the pressure coefficient ($\overline{C}_p$ and $C_{p_{rms}}$, respectively) was computed and presented in Table 2. The correlation heatmap reveals that the main feature that influences the pressure coefficient is α, followed by M, while the correlation with the geometric variation features is minimal, indicating their relatively minor relevance.

Table 2: Correlation heatmap between aerodynamic and geometric features.

	M	α	$\Delta\Lambda$	t/t_0	b/b_0
$\overline{C}_p$	-0.33	-0.92	0.07	-0.08	-0.08
$C_{p_{rms}}$	-0.12	0.93	-0.02	0.02	0.03

The conclusions drawn from the correlation heatmap can be directly linked to the geometric alterations and their impact on the effective Mach number and angle of attack. Modifying the sweep angle, thickness ratio, and span ratio produces effects comparable to altering the local flight condition (M, α). For example, an increase in the sweep angle ($\Delta\Lambda > 0$) results in a reduction of the local Mach number. Similarly, thickening the wing ($t/t_0 > 1$) leads to an increase in the suction peak, thereby promoting stronger shock waves during transonic flight conditions. Conversely, elongating the wing ($b/b_0 > 1$) decreases the induced angle of attack and parasite drag while intensifying compressibility effects,

DOI: 10.13009/EUCASS2023-580

due to a decrease in the sweep near the wing tip, as depicted in Figure 2.

2.2 Model architecture

The core of the surrogate model is the *regressor*, which is designed to predict data for unseen conditions in the training set. In this particular investigation, deep neural networks (DNNs) are proposed as a means to exploit their inherent ability as universal approximators in establishing the nonlinear relationship between design parameters and pressure distributions. The minimal mathematical component of a DNN is the neuron, which acts as a linear function. More than one neuron forms a layer that generates linear values that are transformed using non-linear activation functions applied to each neuron. More than one layer refers to what is called a DNN. These networks then try to approximate, minimising the error between the truth and the predicted value given a loss function implemented in an optimisation algorithm chosen.

The primary objective of this study is to evaluate the performance of a DNN regression model based on a multi-layer perceptron (MLP) composed of various linear layers featuring the rectified linear unit (ReLU) activation function, Maas et al. [16]. The input layer contains 5 neurons, each corresponding to a unique design feature, including flight condition and geometric variations such as $(M, \alpha, \Delta\Lambda, t/t_0, b/b_0)$. Eventually, the MLP produces a vector representing the C_p distribution, with a size equal to the number of grid points.

The MLP architecture is defined to have a total of five layers: an initial layer of five neurons; three hidden layers whose number of neurons increases in size by a factor of 2^4 compared to the preceding layer; and the output layer, with size equal to the dimension of the C_p vector. Consequently, the architecture is structured as $[5, 32, 256, 2\,048, 6\,519]$ and is depicted in Figure 3.

Overfitting the data is a major concern when dealing with fully-connected neural networks trained with a limited amount of data, as is the case. To avoid this undesired phenomenon, a *dropout* with a value of 0.3, is implemented at the fourth layer, Srivastava et al. [17].

Regarding the training process for the MLP, Adam's optimizer is chosen, by Kingma and Ba [18], which is based on a stochastic adaptive process. This method offers the advantage of faster convergence compared to other optimizers, e.g. stochastic gradient descent (SGD) with Momentum by Qian [19]

With respect to the MLP architecture, the correct definition of the regression model is also strongly affected by the hyperparameters that govern the training process. In this study, there are two major hyperparameters that will be taken into consideration for proper tuning of the MLP regressor: the learning rate (l_r), which can be tuned to avoid the possibility of reaching local minima through the non-convex function without exploring for another better minima; and the weight decay (w_d), used to regularise the objective function by preventing large values of the MLP weights and hence avoiding overfitting.

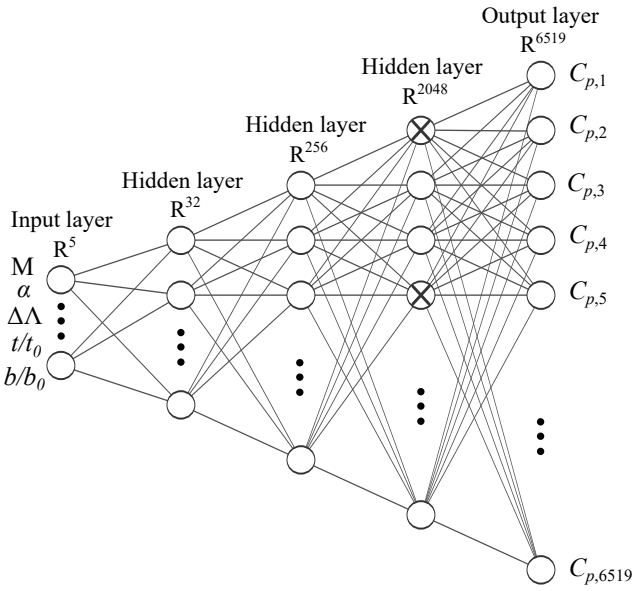

Figure 3: Schematic of the MLP architecture

DOI: 10.13009/EUCASS2023-580

2.3 Robustness analysis on the surrogate model

Despite the prediction performance of the surrogate model, it is also relevant to assess its robustness to fluctuations in the data. Robustness evaluation is based on adding a controlled random noise to the features to determine how the model accomplishes the prediction in terms of error propagation and the confidence interval of the result.

Based on the nature of the data, it was decided to choose a normally-distributed noise with zero mean and a standard deviation based on the uncertainty of each feature, ξ_i, which is estimated as the minimum step between consecutive values from the original distribution of samples (see Table 3). Therefore, a feature F_i will be perturbed with an error E_i such that $F_{i,\text{noise}} = F_i + E_i$ with $E_i \sim N(\mu = 0, \sigma = \varepsilon \cdot \xi_i)$. Note that a tailored scaling factor, ε, is defined to control the noise intensity independently of the uncertainty value. In this study, the robustness to noise will be evaluated for three intensities, namely $\varepsilon = [0, 0.25, 0.50]$.

Table 3: Uncertainty defined for each feature ξ

Features	M	α	$\Delta\Lambda$	t/t_0	b/b_0
ξ_i	0.01	0.5°	1°	0.05	0.05

Robustness analysis relies on the baseline surrogate model, trained without noise, which is subject to perturbations in input data $(M, \alpha, \Delta\Lambda, t/t_0, b/b_0)$. A total of $N = 2\ 500$ samples are tested to guarantee statistical convergence of the process. Finally, this process provides an average estimation of C_p with a confidence interval on the predicted values. Additionally, it is possible to assess the model's robustness to propagate the error by altering the average prediction.

2.4 Hyperparameter tuning of the DNN

The optimisation of the surrogate model will focus on the tuning of two hyperparameters: the learning rate l_r, and the weight decay w_d. The hyperparameter selection process is based on a parametric analysis over a restricted search space summarised in Table 4. A total of 20 combinations of hyperparameters were evaluated targeting the best prediction performance of the DNN. For each combination, the DNN is trained for 10 000 epochs, since, beyond this number, the training loss function ceases to decrease significantly and the test loss function maintains stability with respect to the training loss function, avoiding overfitting.

Table 4: Hyperparameters values used for the cartesian product that formed all the possible combinations for the study on each subset

Hyperparameters	Tested values				
l_r	10^{-1}	10^{-2}	10^{-3}	10^{-4}	
w_d	10^{-1}	10^{-2}	10^{-3}	10^{-4}	10^{-5}

Performance assessment is based on the average mean square error and R^2 metrics for the whole test set. Within the 20 evaluated models, the results for the 5 most performing cases are summarised in Table 5. In terms of hyperparameters, the best combination is $(l_r, w_d) = (10^{-3}, 10^{-5})$. Despite this outcome highlighting the tendency to minimise the weight decay, which implies a reduction in the regularisation of the objective function, there is no evidence of overfitting thanks to the implementation of the dropout as explained above.

Table 5: Ordered global metrics results associated to each model for the subset by the MSE on testing, along with the hyperparameters selected

	Hyperparameters		Metrics results	
Combination	l_r	w_d	MSE ($\times 10^2$)	R^2
1	10^{-3}	10^{-5}	0.97	0.980
2	10^{-4}	10^{-5}	1.12	0.976
3	10^{-3}	10^{-4}	1.97	0.956
4	10^{-4}	10^{-4}	2.21	0.951
5	10^{-2}	10^{-4}	3.33	0.927

DOI: 10.13009/EUCASS2023-580

3. C_p predictions with the surrogate model

In this section, the performance of the trained surrogate model with the best hyperparameter configuration is evaluated, assessing its accuracy in predicting C_p and robustness to noisy data.

The average metrics for the surrogate model, summarised in Table 6, indicate excellent performance as noise has little effect on MSE. These global metrics are calculated as the average MSE and R^2 for all flight conditions included within the test set. Nonetheless, a deeper analysis is required to assess the strengths and weaknesses of the model, since the average, global metrics might hide several interesting pieces of information in that respect. Consequently, the model performance is specifically evaluated in two cases within the test case $C_1 : (M, \alpha, \Delta\Lambda, t/t_0, b/b_0) = (0.86, 6, -2, 1.1, 1.1)$ and $C_2 : (M, \alpha, \Delta\Lambda, t/t_0, b/b_0) = (0.7, 7, 2, 1.1, 1.2)$. These cases represent considerably different scenarios, both highly demanding in terms of the high-α condition together with the presence of shockwaves due to the transonic Mach number.

Table 6: Performance of the MLP for the selected test cases C_1 and C_2 through the comparison between the ground truth and predicted values

						Metrics results					
	Case parameters					$\varepsilon = 0$		$\varepsilon = 0.25$		$\varepsilon = 0.50$	
	M	α	$\Delta\Lambda$	t/t_0	b/b_0	MSE ($\times 10^2$)	R^2	MSE ($\times 10^2$)	R^2	MSE ($\times 10^2$)	R^2
Case C_1	0.86	6	-2	1.1	1.1	0.60	0.988	0.62	0.988	0.63	0.988
Case C_2	0.7	7	2	1.1	1.2	1.70	0.978	1.75	0.978	1.80	0.978
– Average on test set –						0.97	0.980	1.00	0.978	1.12	0.975

Regarding noise robustness, the performance of the surrogate model tends to slightly decay as the intensity of the perturbations grows. Specifically, in C_1, the MSE increases from 0.60 to 0.63, while in C_2, it increases from 1.70 to 1.80, suggesting that the distributions are not entirely normal. Although this result is expected, it is surprising that the global metric is not strongly affected by this noise inclusion into the features of the data. Hence, and for the sake of brevity, the following analysis will only focus on the most demanding scenario, corresponding to $\varepsilon = 0.5$.

Based on a local analysis, Figures 4 and 5 present the chordwise distributions of C_p at different wing spans (η) for values obtained from the CFD simulation, the surrogated model values and the 95% confidence interval of the value distribution using a noise scaling factor of ε_{50}, along with its mean in (a, b, c). Additionally, the subfigure (d) of each case displays the prediction values of the upper surface of the wing.

Figure 6 provides a global perspective as a grid structure. Subfigures (a,c) of the grid show the prediction error ($C_{p\_true} - C_{p\_pred}$) between the CFD simulation values and the prediction results obtained from the surrogate model without any noise scaling factor for each case. The subfigures (b, d) depict the standard deviation of the distribution when a noise scaling factor of ε_{50} is applied to those cases.

Through the results of the case C_1 in Figure 4, it can be seen in subfigures (a) and (c), that abrupt pressure changes at the trailing edge, due to the shock wave, causes the predictor to not be able to capture them, leading to a bias. This prediction flaw underestimates the intensity of the shock wave and shows that the increase in C_p occurs gradually and not abruptly, as observed in the simulations. Along the areas of the chord that are not affected by the shock wave, it can be seen how the prediction leads to a good outcome staying close to the C_p values of the test. While it is true the good behaviour of the prediction, in subfigure (c) we can observe how around 0.5 x/c a pressure drop appears which, although it is not well represented by the prediction, the general trend in that zone is well captured.

For the values obtained from a noise scaling of ε_{50} applied to the features, the mean of the distribution falls closely over the predicted results with zero noise applied. By analysing the 95% confidence interval across the subfigures (a, b, c), apart from the shock wave, the values of the CFD simulation fall within this interval. However, in subfigures (a) and (b), it can be seen that although the value of the confidence interval grows considerably in the shock wave region, it still does not include the Cp values from the simulation.

Analysing Figure 6, in subfigure (a) it can be seen how the largest error in the prediction is committed at the trailing edge of the root and tip where the shock wave appears. In the middle area where the wing is free of shock waves, near the trailing edge, the predicted C_p is slightly more negative than the one obtained in the simulation. On the remaining upper surface, the prediction is in agreement with the values of the test case. In subfigure (b) the deviation grows very significantly in the areas where the shock wave appears, indicating that small variations in the inputs have a significant effect on the prediction of the shock wave effects. It is also interesting to mention how far from the trailing edge the deviation grows gradually from the root towards the wing tip.

DOI: 10.13009/EUCASS2023-580

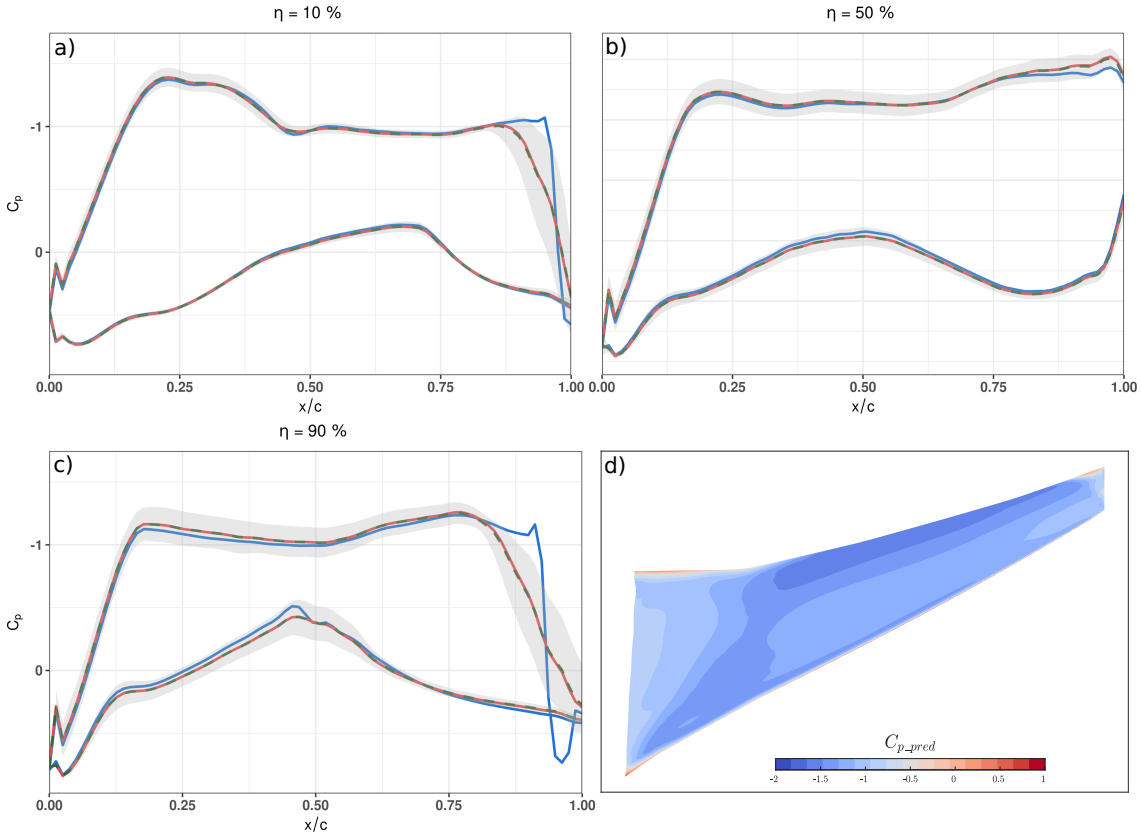

Figure 4: Prediction for C_1. C_p chordwise profiles at $\eta = 0.1$ (a), $\eta = 0.5$ (b) and $\eta = 0.9$ (c), comparing the CFD data (–), prediction with $\varepsilon = 0$ (–), average prediction with $\varepsilon = 0.5$ (– –) and 95% confidence interval (▬). (d) Predicted C_p over the wing upper surface with $\varepsilon = 0$.

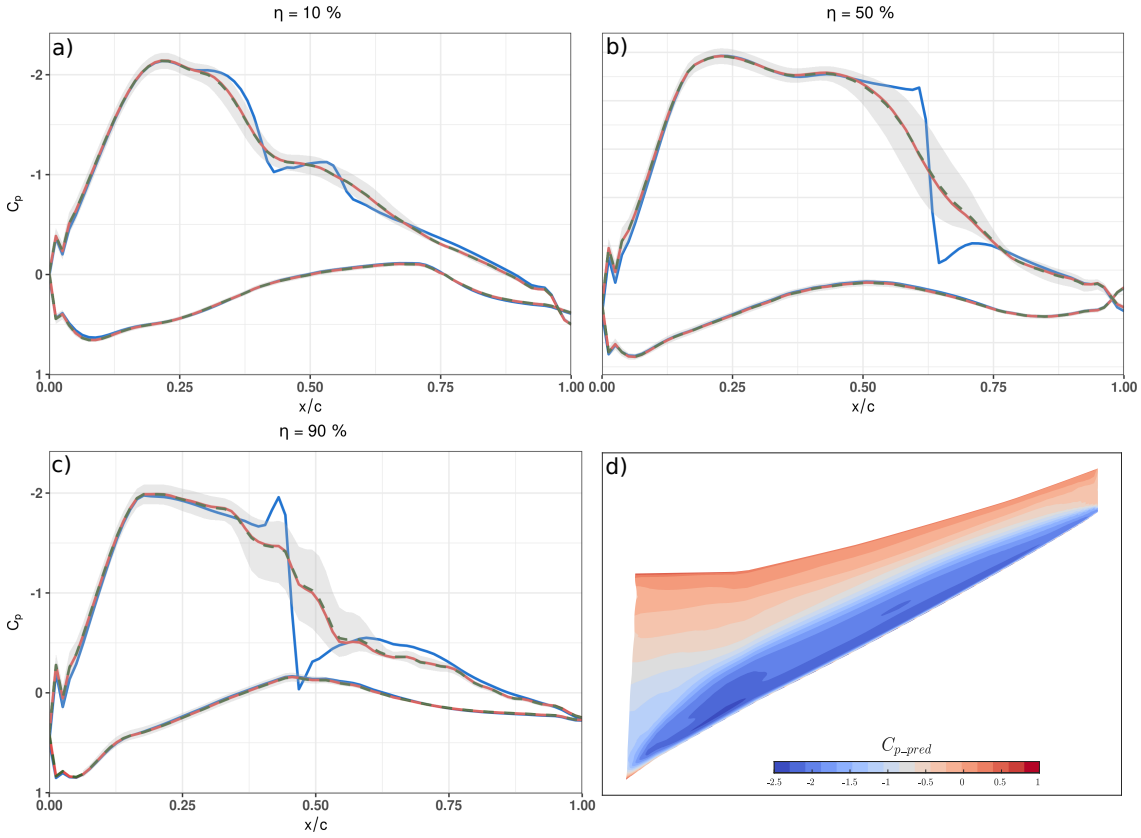

Figure 5: Prediction for C_2. C_p chordwise profiles at $\eta = 0.1$ (a), $\eta = 0.5$ (b) and $\eta = 0.9$ (c), comparing the CFD data (–), prediction with $\varepsilon = 0$ (–), average prediction with $\varepsilon = 0.5$ (– –) and 95% confidence interval (▬). (d) Predicted C_p over the wing upper surface with $\varepsilon = 0$.

DOI: 10.13009/EUCASS2023-580

Concerning to the case C_2 in Figure 5, the presence of a shock wave across the upper side of the wing negatively affects the prediction performance. In general we can see how for the three η the C_p prediction correctly represents the values of the test case on the lower surface while on the upper surface large errors are made. Going to detail, in subfigure (a) we can see how the prediction fails after the suction peak, misrepresenting the posterior pressure rise and the small shock wave that appears in the middle of the chord. As discussed in the previous case, the model is able to predict the general trend but does not correctly adjust for local changes in C_p. In the subfigures (b, c) it can be clearly seen how the prediction of the shock wave cannot follow the continuity in C_p generated by the shock wave, instead depicting a progressive increase in pressure. It is also noteworthy how in subfigure (c) some oscillations appear in the prediction. The effect of the smooth pressure rise in the shock wave can be seen in subfigure (d) where there is no abrupt colour change from the most negative to the most positive values.

In the analysis of the prediction obtained by noise injection, the mean of the distribution is closely aligned with both the CFD simulation values and the predictions without any noise applied. Furthermore, the 95% confidence interval of the lower surface is very narrow. Similarly to case C_1, the confidence interval is capable of capturing most of the C_p values of the simulation in areas where no shock wave appears, but it is unable to capture the abrupt pressure rise after the shock wave. In subfigure (c) of Figure 6 it can be clearly seen how in the shock wave prediction the pressure rise starts before the shock wave appears in the simulation (intense blue area) and how, once it appears, the prediction indicates a lower value of C_p (intense red area) until the error practically disappears away from the shock wave. In subfigure (d) shows that the deviation in the shock wave area is much larger than in the rest of the wing, indicating the lack of stability in the prediction in that region in the presence of noise in the inputs.

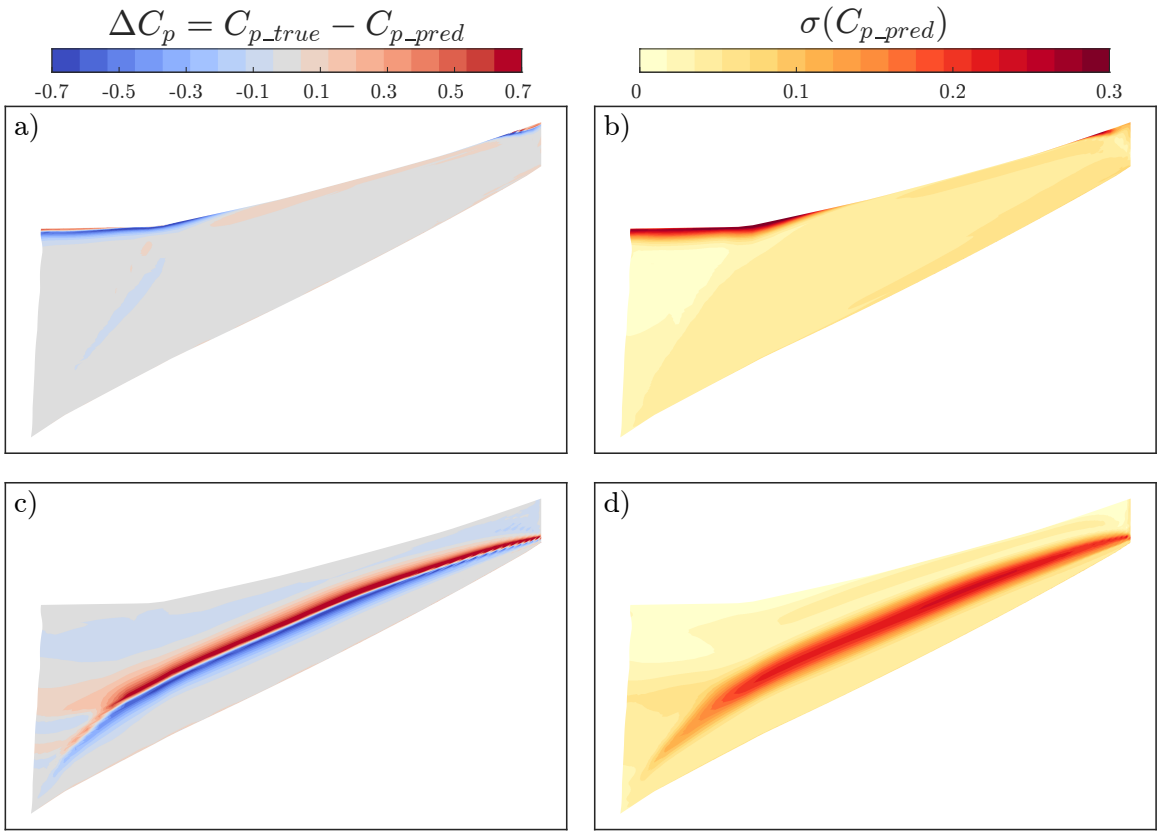

Figure 6: Distribution over the upper wing surface of the prediction error and standard deviation for C_1 (first row) and C_2(second row) using predicted C_p where ε =50.

4. Conclusions

This article assesses the performance of a DNN by applying it to a database consisting of CFD simulations of a wing in a transonic regime. The aim is to predict pressure coefficients based on various flight conditions and geometric parameters. This database also contains shock waves, which pose an additional difficulty to be taken into account when evaluating. In order to assess the behaviour of the models under these conditions, a neural network architecture has

DOI: 10.13009/EUCASS2023-580

been defined and its robustness to different changes in the input values has been analysed through the generation of new inputs from the application of a normally-distributed noise to each of them.

The results show that the most suitable values for the explored hyperparameters set of $[l_r, w_d]$ are $[10^{-3}, 10^{-5}]$ respectively, which leads to an average MSE of 0.0097. After training the model, the application of noise scaling to the features which goes up to 50%, increases the average MSE of the test set by 13%. The analysis of two selected cases from the *test* set, which involve challenging shockwave effects, reveals some differences between the CFD simulations and the predicted values. As shown, the predicted C_p values have a very low error globally; however, this error grows considerably in the shock wave. It has been seen that systematically the instantaneous pressure climb after the shock wave is not well captured by the model, transforming it into a smooth rise of C_p that is not consistent with the physics of the problem.

The different ε applied to the features in both cases demonstrates that the distribution of prediction values deviates slightly from a normal distribution, although the input features were generated from one. Regarding the 95% confidence interval obtained, it should be noted that, despite the high error introduced in the inputs, the margin obtained is narrow in the majority of the wing surface, indicating good stability of the model to predict noisy inputs. However, in areas that show the shock wave, this confidence margin widens markedly, suggesting that the predicted position of the shock wave and its intensity are sensitive to small changes in the values of the features. This information on noise stability could be used in the future to pinpoint specific areas where more data are needed to better understand trends.

The presented model achieves accurate predictions within the subsonic regime, displaying consistent alignment with the true C_p values along the entire wing, being able to be used directly for wings operating at relatively low speeds. However, the model is not able to correctly predict the shock waves, so it would not be suitable for the transonic regime. This is a problem to be further explored, where an starting point, could be the use of Reduce Order Models (ROMs) such as Isomap, to reduce complexity while maintaining its intrinsic characteristics. In addition, the use of explainability techniques can lead to better treatment of the data, while allowing a deeper understanding of various parameters and ultimately improving the effectiveness of the model.

Acknowledgments

The authors thank Airbus for providing the database for the XRF1 test case.

References

[1] R. Yondo, K. Bobrowski, E. Andrés, and E. Valero. A review of surrogate modeling techniques for aerodynamic analysis and optimization: current limitations and future challenges in industry. *Advances in evolutionary and deterministic methods for design, optimization and control in engineering and sciences*, pages 19–33, 2019.

[2] E. Andrés and Carlos Paulete-Periáñez. On the application of surrogate regression models for aerodynamic coefficient prediction. *Complex & Intelligent Systems*, 7(4):1991–2021, Aug 2021. ISSN 2198-6053.

[3] H. Moin, H.Z.I. Khan, S. Mobeen, and J. Riaz. Airfoil's aerodynamic coefficients prediction using artificial neural network. In *2022 19th International Bhurban Conference on Applied Sciences and Technology (IBCAST)*, pages 175–182. IEEE, aug 2022.

[4] K. Yonekura and K. Suzuki. Data-driven design exploration method using conditional variational autoencoder for airfoil design. *Structural and Multidisciplinary Optimization*, 64(2):613–624, Aug 2021. ISSN 1615-1488.

[5] J. Li, M. Zhang, J. R.R.A. Martins, and C. Shu. Efficient aerodynamic shape optimization with deep-learning-based geometric filtering. *AIAA Journal*, 58(10):4243–4259, 2020.

[6] S. Cheng, C. Quilodrán-Casas, S. Ouala, A. Farchi, C. Liu, P. Tandeo, R. Fablet, D. Lucor, B. Iooss, and J. Brajard. Machine learning with data assimilation and uncertainty quantification for dynamical systems: a review. *IEEE/CAA Journal of Automatica Sinica*, 10(6):1361–1387, 2023. ISSN 2329-9266.

[7] G. Shahzadi and A. Soulaïmani. Deep neural network and polynomial chaos expansion-based surrogate models for sensitivity and uncertainty propagation: an application to a rockfill dam. *Water*, 13(13):1830, 2021. ISSN 2073-4441.

[8] M. Abdar, F. Pourpanah, S. Hussain, D. Rezazadegan, L. Liu, M. Ghavamzadeh, P. Fieguth, X. Cao, A. Khosravi, and U.R. Acharya. A review of uncertainty quantification in deep learning: Techniques, applications and challenges. *Information Fusion*, 76:243–297, 2021. ISSN 1566-2535.

DOI: 10.13009/EUCASS2023-580

[9] V. Ziyadinov and M. Tereshonok. Noise immunity and robustness study of image recognition using a convolutional neural network. *Sensors*, 22(3):1241, 2022. ISSN 1424-8220.

[10] I.B.V. Silva and P.J.L. Adeodato. Pca and gaussian noise in mlp neural network training improve generalization in problems with small and unbalanced data sets. In *The 2011 International Joint Conference on Neural Networks*, pages 2664–2669. IEEE, 2011.

[11] A. Camuto, M. Willetts, U. Simsekli, S.J. Roberts, and C.C. Holmes. Explicit regularisation in gaussian noise injections. *Advances in neural information processing systems*, 33:16603–16614, 2020.

[12] GARTEUR AD/AG-60 Machine learning and data-driven approaches for aerodynamic analysis and uncertainty quantification. `https://garteur.org/`. Accessed: 2023-03-08.

[13] R Castellanos, J. Nieto-Centenero, A. Gorgues, S. Discetti, A. Ianiro, and Andrés E. Towards aerodynamic shape optimisation by manifold learning and neural networks. Chania, Crete, Greece, 06 2023. ECCOMAS.

[14] V.E. Kovalev and O.V. Karas. Calcul de l'écoulement transsonique autour d'une configuration aile-plus-fuselage compte tenu des effects visqueux et d'une région décollée mince. *La Recherche. Aérospatiale*, (1):23–38, 1994.

[15] K. Zhang and M. Hepperle. Evaluation of the BLWF Code - A Tool for the Aerodynamic Analysis of Transonic Transport Aircraft COnfigurations. Technical report, Institut für AeroDynamik und Strömungstechnik, Juli 2010.

[16] A.L. Maas, A.Y. Hannun, and A.Y. Ng. Rectifier nonlinearities improve neural network acoustic models. In *Proc. icml*, volume 30, page 3. Atlanta, Georgia, USA, 2013.

[17] N. Srivastava, G. Hinton, A. Krizhevsky, I. Sutskever, and R. Salakhutdinov. Dropout: a simple way to prevent neural networks from overfitting. *The journal of machine learning research*, 15(1):1929–1958, 2014. URL `http://jmlr.org/papers/v15/srivastava14a.html`.

[18] D.P. Kingma and J. Ba. Adam: A method for stochastic optimization. *arXiv preprint arXiv:1412.6980*, 12 2014.

[19] N. Qian. On the momentum term in gradient descent learning algorithms. *Neural networks*, 12(1):145–151, 1999. ISSN 0893-6080.